J. of Supercritical Fluids 81 (2013) 175–182

Contents lists available at SciVerse ScienceDirect

The Journal of Supercritical Fluids

journal homepage: www.elsevier.com/locate/supflu

In situ monitoring of the adsorption of Co^{2+} on the surface of Fe_3O_4 nanoparticles in high-temperature aqueous fluids

Hao Yan[a,*], Robert A. Mayanovic[a], Joseph W. Demster[a], Alan J. Anderson[b]

[a] Department of Physics, Astronomy and Materials Science, Missouri State University, Springfield, MO 65897, USA
[b] Department of Earth Sciences, St. Francis Xavier University, P.O. Box 5000, Antigonish, Nova Scotia B2G 2W5, Canada

ARTICLE INFO

Article history:
Received 20 December 2012
Received in revised form 6 May 2013
Accepted 23 May 2013

Keywords:
Nanostructures
Oxides
Surfaces
XAFS
Adsorption
Electron microscopy

ABSTRACT

Developing an understanding of the reaction processes occurring at the surface–fluid interface at the atomic level of nanostructured materials in high-temperature aqueous environments is necessary for establishing general principles of behavior of nanomaterials operating in such extremes. In situ Co *K*-edge X-ray absorption spectroscopy (XAS) measurements were made on Fe_3O_4 nanoparticles in the presence of Co^{2+} ions in aqueous fluids to 500 °C and approximately 220 MPa. The results from analysis of the in situ EXAFS data, along with SEM-EDX spectra measured from reacted nanoparticles, indicate that adsorption of Co^{2+} ions on the surface of Fe_3O_4 nanoparticles is negligible at temperatures below 200 °C but becomes significant in the 250–500 °C temperature range. The low reaction temperature threshold of the Co^{2+} aqua ion with Fe_3O_4 nanoparticles is consistent with a relatively low value of the crystal field stabilization energy (CFSE) of Co^{2+} in octahedral site symmetry in spinels. Modeling of the pre-edge feature of the XANES and analysis of the extended X-ray absorption fine structure (EXAFS) shows that Co^{2+} adsorbs predominantly on octahedral sites of the surface of nanoparticles in aqueous fluids. Structural analyses using EXAFS and high resolution TEM show that the inverse spinel structure is preserved in the Co-incorporated surface atomic layers of the Fe_3O_4 nanoparticles. Our results suggest that the dissolved radioactive isotope ^{60}Co in the primary cooling loop of supercritical water-cooled nuclear reactors have a high likelihood of precipitating on the surfaces of spalled ferrite nanomaterial.

1. Introduction

Oxide-based nanomaterials are projected to play a significant role in the conversion and storage of energy under extreme P–T–γ conditions (P: pressure, T: temperature, and γ represents ionizing electromagnetic and particle radiation) including in supercritical aqueous environments. For increased efficiency, next-generation conventional and nuclear power reactors are projected to operate with pure water at supercritical conditions (beyond 374 °C and 22.06 MPa) thereby increasing the potential for oxidation and corrosion of materials in the primary loop [1,2]. The spalling of nanoparticulate material including ferrite nanoparticles, that results from the oxidation and corrosion of steel-alloyed pipes and reactor vessel walls of primary cooling loops, is a potentially critical-failure issue in supercritical water-cooled power reactors (SCWRs). For example, collection of spalled material at tube bends and joints may result in overheating and rupture of pipes in the primary loop or the rapid transport of spalled byproducts upon reactor startup may result in erosion damage in the steam turbine and main steam valves in SCWRs. In addition, the spalled ferric nanoparticles are transported along with corrosion-product metal ions, such as Fe^{3+}, Ni^{2+}, Co^{2+}, and Cr^{3+}, in the supercritical water-cooled power reactors (SCWRs) [1,3,4]. The fate of the corrosion-product metal ions is an issue because these lower the pH and enhance the corrosiveness of the fluid within the primary cooling loop [5]. It has also been proposed that coating of the interior of the pipes and reactor vessel walls of the primary cooling loops with metal oxide nanoparticulate material may reduce the corrosion and oxidation in SCWRs [6,7]. Data on the reactivity of spalled ferrite nanoparticles with corrosion-product metal ions and on the structural stability of metal oxide nanoparticulate coatings in the supercritical fluids of SCWRs are not widely available. Along with the structural and magnetic properties, the solubility and reactivity of ferrite nanoparticles can be modified and/or altered by chemisorption of the metal ions on the nanoparticles, depending upon the chemical makeup of the fluid and upon the thermodynamic conditions of the system. Formulating an understanding of the physical and chemical processes occurring at the atomic level on the surface of nanomaterials in supercritical aqueous fluids is vital for developing the knowledge of reactor chemistry and materials required to design the next generation of reactors. In situ monitoring of nanoparticles in metal-ion-bearing

* Corresponding author. Present address: Center for High Pressure Science and Technology Advanced Research, 1690 Cailun Rd, Pudong, Shanghai 201203, P.R. China. Tel.: +1 417 836 5132; fax: +1 417 836 6226.
E-mail addresses: HaoYan@missouristate.edu, yanhao@hpstar.ac.cn (H. Yan).

0896-8446/$ – see front matter © 2013 Elsevier B.V. All rights reserved.
http://dx.doi.org/10.1016/j.supflu.2013.05.017

aqueous fluids to supercritical conditions is efficient because it avoids multiple bench-top experiments and samples and it is highly valuable because it enables direct study of the nanoparticle surface–fluid interface. Because of current interest in surface doping of nanoparticles for catalysis applications where cost is a factor, particularly with precious metals or rare earth elements, the knowledge gained from this study should also prove useful for hydrothermal synthesis of nanostructured materials.

Aside from having unique catalytic, electrical and optical properties, ferrite nanoparticles may exhibit unusual magnetic properties that are not observed in their bulk counterparts, such as superparamagnetism and quantum tunneling of magnetization, provided the mean particle size is sufficiently small. These properties are typically dependent upon the size, morphology, and shape of the nanoparticles. Spinel ferrite nanoparticles of varied compositions are particularly interesting for investigations of the dependence of magnetic properties on the elemental constituents and structure. Spinel ferrite nanoparticles have proven useful as contrast enhancers in magnetic resonance imaging [8] and for site-specific drug delivery [9] and show promise for hyperthermia therapy [10], ferrofluid, and information storage media applications. The chemical formula of magnetite, which is an inverse spinel-structured ferrite, can be expressed as $Fe^{II}Fe^{III}{}_2O_4$. The oxygen atoms occupy the close-packed face-centered cubic cell lattice sites whereas 8 tetrahedral (A) sites are occupied by Fe^{3+} ions and 16 octahedral (B) sites are occupied evenly by Fe^{3+} and Fe^{2+} ions. The general formula of spinel ferrites is MFe_2O_4 (M = Mg, Mn, Co, Ni, Zn, etc.). The structure of spinel ferrites ranges from normal to inverse spinel, depending upon the precise distribution of the M and Fe atoms on the cation sublattice [11]. The degree of inversion of a generic spinel ferrite can be formulated as $[M_{(1-i)}Fe_i]^A[M_iFe_{(2-i)}]^BO_4$, where i is the inversion parameter having values of 0 for a normal spinel, 1 for a fully inverse spinel, and intermediate for a partially inverse spinel structure [12]. Bulk $CoFe_2O_4$, which has direct relevance to this study, has been shown to be an inverse spinel [13].

In our previous study, we investigated the temperature-dependent structural properties of Ni^{2+} ions reacting with Fe_3O_4 nanoparticles in aqueous fluids to supercritical conditions [14]. Our results indicate that the reactivity of Fe_3O_4 nanoparticles with Ni^{2+} ions is negligible to 300 °C but becomes significant in the 400–500 °C temperature range and that the Ni^{2+} adsorbs predominantly on octahedral sites of the surface of nanoparticles. Due to the short-range order of structure of Ni chemisorbed on the surface of the nanoparticles in the aqueous system, XAS was demonstrated to be ideally suited for the study. Through a combination of analyses of the extended X-ray absorption fine structure (EXAFS) and X-ray absorption near edge structure (XANES) of XAS, detailed information was obtained on the local structure and chemical nature of Ni^{2+} ions adsorbed on Fe_3O_4 nanoparticles [14]. The goal of our in situ XAS investigation presented herein is to examine the structural and chemical (i.e., at the Co valence state) properties surrounding the Co^{2+} ion, at the fluid-Fe_3O_4 nanoparticle interface, and to determine how these properties depend upon P–T conditions. Furthermore, we aim to compare the structural and chemical properties of Co with Ni upon chemisorption on Fe_3O_4 nanoparticles in high-temperature aqueous fluids.

2. Experimental

2.1. Sample preparation

Identical Fe_3O_4 nanoparticles (NPs) used in our previous study of Ni^{2+} ions adsorbed on Fe_3O_4 NPs in high P–T aqueous solutions were used to prepare the samples for this study [14]. As reported previously, XRD measurements of the nanoparticles used in sample preparation showed they were Fe_3O_4 phase and use of Gaussian fitting and the Scherrer equation showed the estimated size of the nanoparticles to be ca. 24 nm [15].

The 0.05 m $Co(NO_3)_2$ aqueous solution was prepared from commercially available cobalt nitrate powder (GFS Chemicals) and nitrogen-deoxygenated deionized water. The solution was clear without any presence of a hydroxide precipitate. The sample was made by mixing 0.232 g iron oxide NPs and 5 ml 0.05 m $Co(NO_3)_2$ aqueous solution (Co-Fe_3O_4 NP•aq sample). Our calculations show that the molar ratio of Co^{2+}/surface site < 1, where we assume only octahedral site occupation of Co^{2+} on Fe_3O_4 NP and spherical shape of the nanoparticles. This ensures maximum XAS signal quality with negligible coexistant aqueous Co^{2+} species once Co is fully adsorbed on Fe_3O_4 NPs under high P–T conditions in the sample. The sample was sonicated for 10 min prior to loading a small amount into the hydrothermal diamond anvil cell (HDAC) for the experiments. The pH value of the sample measured at room temperature was 4.96.

2.2. Scanning electron microscopy and high resolution transmission electron microscopy

An FEI Quanta 200 instrument, operating at 30.0 kV, was used for Scanning Electron Microscopy (SEM) imaging and energy-dispersive X-ray (EDX) spectroscopic analyses of the NP samples. The EDX analysis was performed on the samples using a Field Emission Gun (FEG). As was the case for our study of Ni^{2+} ions adsorbed on Fe_3O_4 NP in aqueous solution to high P–T conditions [14], the same $Co(NO_3)_2$ + Fe_3O_4 NP aqueous solution samples were heated in our hydrothermal reactors to similar P–T conditions as in the HDAC for additional characterization. Hydrothermally treated Co-Fe_3O_4 and untreated Fe_3O_4 NPs powder dried at room temperature and attached on a conductive carbon tape were observed with the SEM.

To prepare the samples for High Resolution Transmission Electron Microscopy (HRTEM), Fe_3O_4 NPs were dispersed in hexane at room temperature and sonicated for 15 minutes. Subsequently, a drop of nanoparticle suspension in hexane was evaporated on holey TEM grids. An FEI Tecnai F20 STEM operating at 200 kV was used to obtain HRTEM images of the Fe_3O_4 NPs.

2.3. Synchrotron XAS measurements

The synchrotron XAS measurements were made on the Co-Fe_3O_4 NP•aq sample loaded in a Bassett-type HDAC. The design of the HDAC has been described previously by our group [16–18]. Briefly, the HDAC consists of an upper diamond anvil with a flat culet face and a lower diamond anvil with a 300 μm-diameter and 80 μm-depth sample recess situated in the center of the culet face. No gasket was used between the anvils to avoid possible contamination and non isochoric behavior of the fluid sample because of gasket corrosion and deformation under high P–T conditions. The lower anvil has two milled grooves leading to the sample recess, to reduce the attenuation of the incident X-rays and the signal fluorescence. The sample was loaded into the recess of the lower diamond and sealed, together with a vapor bubble, against the upper diamond anvil. During the loading of the sample, a minor amount of O_2 is present in the vapor but this is negligible in relation to the amount of Co and Fe_3O_4 NPs in the aqueous phase of the sample. Once heated, the pressure in the sample increases along the liquid–vapor curve to the P–T point where complete miscibility between the liquid and vapor phase is achieved. The complete miscibility point is characterized by the homogenization temperature (T_h), which is recorded via direct observation of the sample during heating using a video camera and microscope. The T_h value is directly dependent upon the sample density. Upon further heating above T_h, the sample pressure moves beyond the liquid–vapor

curve and increases along an isochore determined by the density (and T_h value) of the sample. Sample pressures along the isochore were calculated from the equation of state of water [19] using the measured density and temperature values. The estimated error in pressure is 3%.

Co *K*-edge XAS measurements were made on the Co-Fe_3O_4 NP•aq samples at the PNC/XOR beam line 20-ID-B of the Advanced Photon Source (APS). About 71% volume of the HDAC recess was filled with the sample and the remaining volume consisted of a vapor bubble (i.e., the sample density was 0.71 g/cm^3). The sample pressure varied from vapour pressure (close to atmospheric) at 25 °C to ~ 220 MPa at 500 °C. The HDAC was oriented with its compression axis vertically, at perpendicular orientation to the incident X-ray beam. The sample was heated from a lower to a higher measurement *P*–*T* point at a rate of 10 °C/min. A 4-element Vortex detector, placed horizontally at 90° orientation to the incident micro-focused (ca. 4–5 μm dia.) X-ray beam, was used to measure the fluorescence XAS spectra. The synchrotron was operated at 7.0 GeV and 100 mA maximum fill current. The incident X-ray beam flux was 1×10^{11} photons/s. Co *K*-edge calibration was accomplished using cobalt metal foil. In addition, commercially available $CoFe_2O_4$ powder (Alfa Aesar) was used for comparative Co *K*-edge XAS measurement purposes.

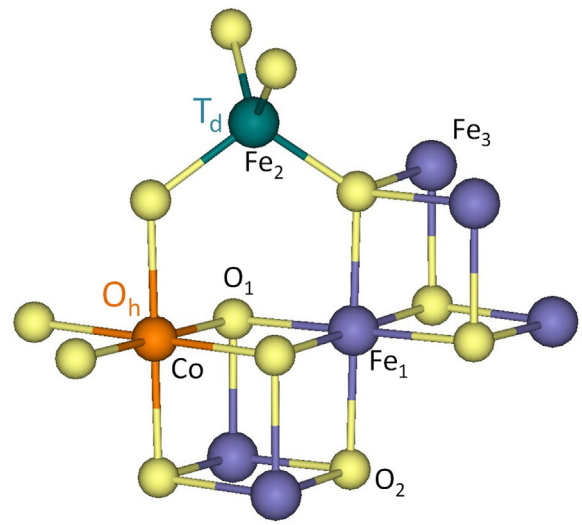

Fig. 1. An atomic model showing part of the Fe_3O_4 based cluster used for theoretical FEFF calculations of XANES and EXAFS. The Co ion was situated alternately in octahedral (O_h) or tetrahedral (T_d) site of the atomic cluster.

2.4. XANES data analysis

XANES calculations were carried out using the FEFF8.2 code [20]. The atomic model used in the calculations consists of a central Co atom substituting for one of the octahedrally (O_h) or tetrahedrally coordinated (T_d) Fe atoms within a cluster of atoms based on the magnetite (Fe_3O_4) structure (seen Fig. 1). Modeling of the in situ Co *K*-edge XANES, including the calculation of the associated angular momentum projected density of states (*l*-DOS), beyond the pre-edge region of the adsorbed Co^{2+} ion on the Fe_3O_4 NPs using FEFF8.2 was examined in our previous work [21]. We found that it is not possible to fit the pre-edge and the remainder of XANES simultaneously using FEFF code; however, this can be accomplished in parts. Following the approach used to model the pre-edge features of Mn-bearing oxide compounds [22], the metal atoms were removed leaving only the central Co and oxygen atoms in the atomic clusters used in XANES calculations. Atomic clusters up to three immediate neighboring shells of oxygen atoms surrounding the Co atom were used for the pre-edge XANES calculations. Self-consistent field (SCF) potential calculations in full multiple scattering mode were used. Hedin–Lundqvist [23] potentials were used in the XANES calculations. Values ranging from 0.6 eV to 0.8 eV in dispersion were used to account for instrument and core-hole lifetime broadening. A default AFOLP value (1.15) was used to overlap and thereby reduce discontinuities between adjacent regions of muffin-tin potentials used in the calculation. The mean square relative disorder parameter of the Debye–Waller factor was set at 0.010 Å^{-1}.

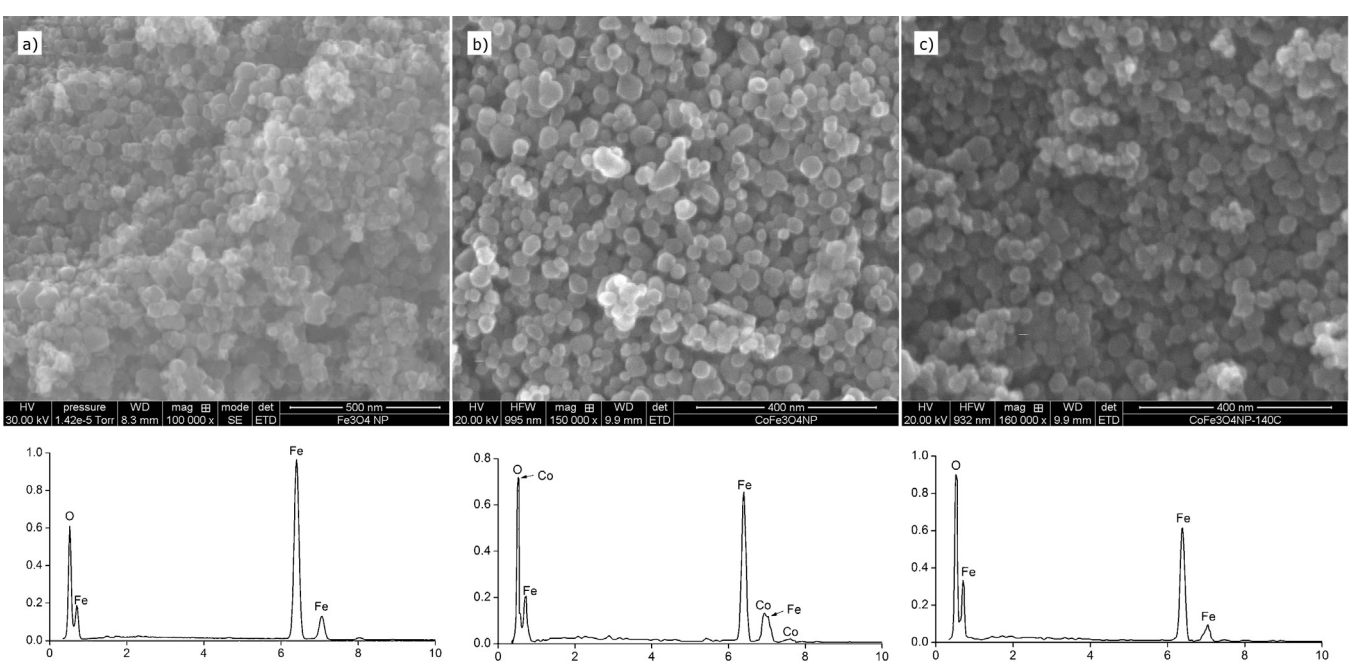

Fig. 2. SEM images taken of (a) Fe_3O_4 NPs, (b) Fe_3O_4 NPs reacted in aqueous fluids with Co to 370 °C, and (c) Fe_3O_4 NPs reacted with Co to 140 °C. Below each SEM image are shown the respective SEM-EDX data.

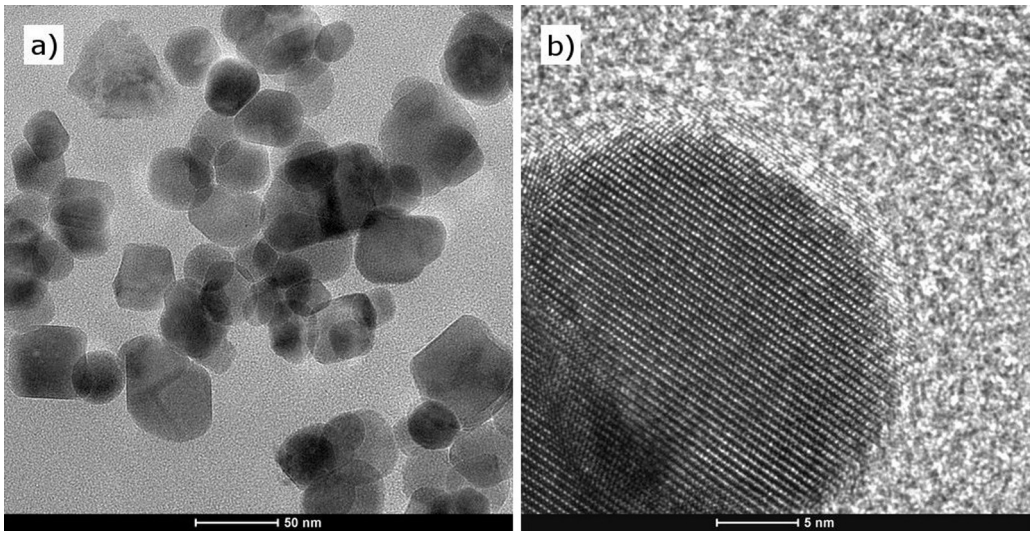

Fig. 3. High resolution TEM images taken at (a) 71,000 times magnification of Co-Fe_3O_4 NPs and at (b) 690,000 times magnification of an individual Co-Fe_3O_4 NP reacted in aqueous fluids to 370 °C.

2.5. EXAFS data analysis

Prior to reduction of the XAS spectra, the Bragg peaks from the diamond anvil were removed from each spectrum using the procedures outlined elsewhere [16]. An average of up to five individual spectra measured at a single *P–T* point were analyzed. It should be noted that there was relatively minor change in the spectra with time and, therefore, the averaged spectra represent an average over time for fixed *P–T* of the sample. The XAS spectra were reduced using ATHENA0.8 software [24] and fitting of the χ data was made using a nonlinear least squares algorithm within the IFEFFIT0.9 software package [25]. The k^3-weighted Co *K*-edge χ data were then Fourier transformed in k-space from a minimum value of 0.5 $Å^{-1}$ to a maximum value of 10.5 $Å^{-1}$. Fitting was made of the Fourier-tranformed χ data over the *R*-space range 0.9–3.7 Å.

The χ data were fit in *R*-space with theoretical XAS curves generated using the FEFF8.2 program [20]. FEFF8.2 is an ab initio curved wave multiple scattering XAS theory incorporating many body effects. A cluster model containing up to 25 atoms based on the structure of spinels (i.e., spinel-motif) was used to calculate theoretical XAS curves using FEFF8.2. The target or central atom (Co) is located at one of the metal sites, at one end of the cluster model, to structurally simulate the adsorption of the Co^{2+} ion on the surface of a Fe_3O_4 NP in the aqueous fluid at high *P–T* conditions. In up to 140 single and multiple scattering paths generated using the cluster models described above and FEFF8.2, four single scattering paths (Co ↔ O and Co ↔ Fe) were used in fitting of the Co *K*-edge χ data. For each path, the set of parameters used in the fitting of the χ data included the coordination number (*N*), the radial distance (*R*), the mean square relative displacement (σ^2) of the XAS Debye–Waller factor, and ΔE_0, the shift between E_o and its theoretically calculated value. The standard amplitude normalization factor ${S_0}^2 = 0.9$ was used to determine the coordination number *N* of each path used in the fitting.

3. Results and discussion

SEM images in Fig. 2 show that the untreated Fe_3O_4 NPs and the Fe_3O_4 NPs hydrothermally treated in the presence of Co-bearing solutions have roughly the same morphological features. SEM-EDX spectra show that Co ions are adsorbed on the Fe_3O_4 NPs subsequent to hydrothermal treatment to 370 °C (Fig. 2b) and that Co ions are not adsorbed on Fe_3O_4 NPs subsequent to hydrothermal treatment to 140 °C (Fig. 2c). That indicates Co ions are chemisorbed on the Fe_3O_4 NPs subsequent to hydrothermal treatment only at a high enough temperature (e.g. 370 °C), while Co ions are physisorbed at lower temperatures (e.g. 140 °C).

TEM images of the Co-Fe_3O_4 NPs are shown in Fig. 3. Representative TEM images of the nanoparticles indicate a wide size distribution with a mean size consistent with XRD measurements of the Fe_3O_4 NPs prior to hydrothermal treatment in the presence of Co [14]. TEM observation also shows that the Co-Fe_3O_4 NPs are single crystal nanocrystallites.

3.1. XANES

The X-ray absorption near edge structure (XANES) is a sensitive probe of the coordination geometry, bonding environment and electronic structure surrounding the central atom. We have presented a detailed analysis, aside from ab initio modeling of the pre-edge feature presented here, of the Co *K*-edge XANES measured from the Co-Fe_3O_4 NP•aq sample elsewhere [21] and only provide a summary of the results here. From peak-fitting analysis of the overall XANES, it was found that the association between Co^{2+} and Fe_3O_4 NPs is negligible from room temperature to 200 °C but becomes significant from 250 °C to 500 °C, in the low pH aqueous fluid: An example of the Co *K*-edge XANES measured from the Co-Fe_3O_4 NP•aq sample is shown in Fig. 4. The reaction of Co^{2+} ions and Fe_3O_4 nanoparticles was also verified from peak-fitting analyses of the temperature-dependent pre-edge feature occurring in the 7704–7714 eV range of the XANES. The pre-edge feature originates from dipole-allowed transitions of Co 1s-electrons to unoccupied states having mixed 3d (Co) and p (Co, O) character and, to a lesser degree, to quadrupole-allowed 1s → 3d electronic transitions on the Co ion. The background subtracted and normalized pre-edge feature exhibits a single peak from 25 °C to 200 °C, indicating predominant Co^{2+} aqua ion speciation, and a double-peaked feature from 250 °C to 500 °C, indicating adsorption of the Co^{2+} ion on the surface of Fe_3O_4 nanoparticles in the aqueous solution. The double-peaked feature in the pre-edge XANES is indicative of the crystal field (or molecular-orbital) splitting of the Co 3d orbital sub-bands, upon reaction and adsorption of the Co^{2+} ion on the surface of Fe_3O_4 NPs. Our objective in this work is to make a closer examination of the issue of site occupation upon adsorption of the Co^{2+} ion on the Fe_3O_4 NPs using ab initio modeling of the pre-edge feature of the Co *K*-edge XANES data.

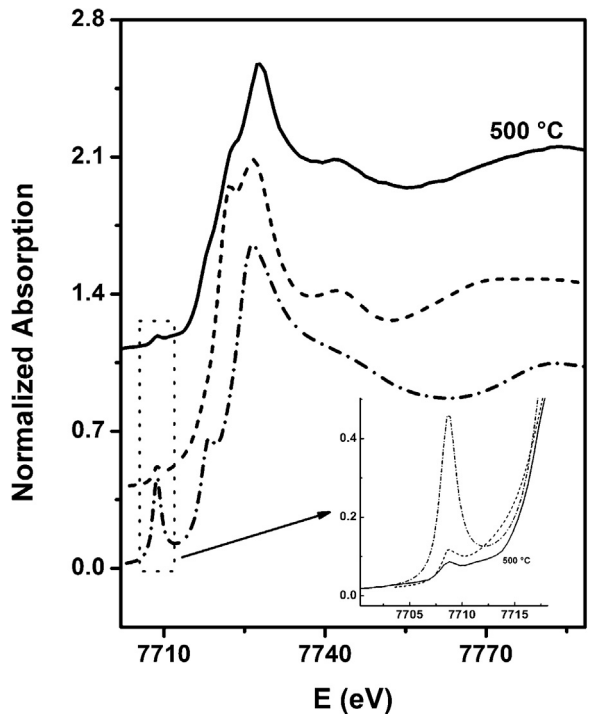

Fig. 4. Modeling of the pre-edge feature located in the vicinity of 7708 eV of the XANES data (solid line) measured from the Co-Fe_3O_4NP•aq sample at 500 °C and 220 MPa using FEFF8.2 and a spinel-based cluster with Co occupying a tetrahedral site (dot dashed line) and an octahedral site (dashed line). The inset shows the pre-edge feature in the same line scheme as indicated above.

In Fig. 4, we compare the calculated XANES using an O_h symmetry cluster of 29 atoms and a T_d symmetry cluster of 27 atoms and the Co *K*-edge XANES measured from the Co-Fe_3O_4 NP•aq sample at 500 °C. Clearly, the calculated spectra are in poor agreement with the measured XANES beyond the pre-edge region due to the missing metal atoms in the cluster. In the pre-edge region however (see inset of Fig. 4), the XANES calculated using an O_h symmetry cluster agrees well with the XANES measured from the sample. Conversely, the XANES calculated using the T_d symmetry cluster is found to have a pre-edge feature of considerably greater intensity than the pre-edge feature in the XANES measured from the sample. The strong intensity of the pre-edge feature in the T_d symmetry is attributed to the lack of centrosymmetry allowing for local mixing (or hybridization) of Co 4p and 3d states [26]. Closer inspection of the calculated pre-edge features indicates that the T_d symmetry cluster has a unimodal (i.e., singlet) appearance whereas the O_h symmetry cluster has a bimodal (i.e., doublet) appearance and is in good agreement with the XANES measured from the sample. Therefore, modeling of the pre-edge feature of the Co *K*-edge XANES measured from the Co-Fe_3O_4 NP•aq sample shows that the Co^{2+} ion occupies the octahedral metal site upon adsorption on Fe_3O_4 NPs.

3.2. EXAFS

The Fourier transforms (FT) of the k^3-weighted Co *K*-edge χ data and the fits of the FT data as a function of *P*–*T* conditions are shown in Fig. 5. In Fig. 6 we show the k^3-weighted inverse Fourier transform ($k^3 \cdot \tilde{\chi}(k)$) data calculated from the FT data shown in Fig. 5 together with the fits to the $k^3 \cdot \tilde{\chi}(k)$ data. For comparative purposes only, we also show the fit of the Co *K*-edge EXAFS data (in Figs. 5 and 6) measured from a $CoFe_2O_4$ bulk powder sample in transmission mode. The FT and the $k^3 \cdot \tilde{\chi}(k)$ data indicate that the reactivity is minimal at low temperature and the Co^{2+} ions have predominantly aqua ion coordination at 25 °C and up to 200 °C.

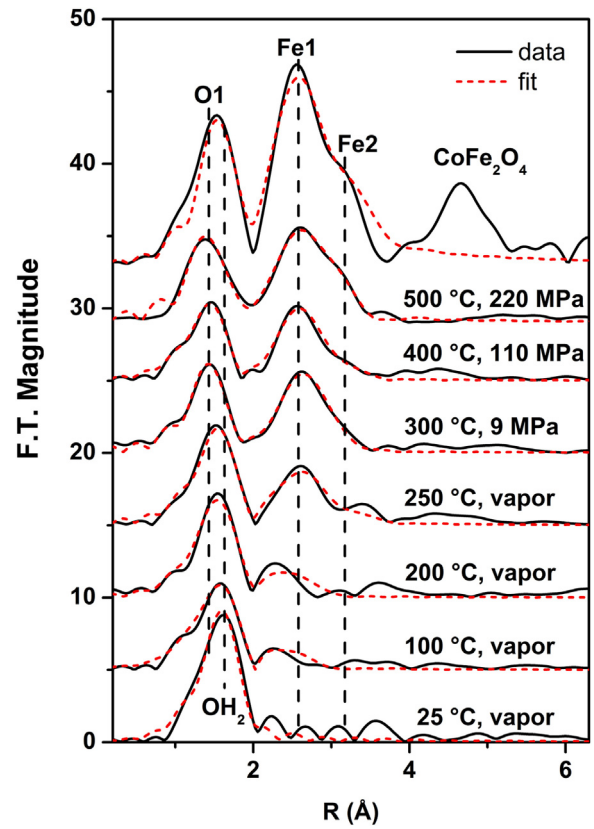

Fig. 5. Magnitude of Fourier transforms (FT) of the $k^3 \cdot \chi(k)$ data (solid lines) obtained from the EXAFS spectra of the Co-Fe_3O_4 NP•aq sample measured from 25 °C to 500 °C and vapor pressure to 220 MPa and from bulk $CoFe_2O_4$. The corresponding best fits to the Fourier transform data are shown as dashed lines. Note the changeover of the features in the FT data indicating a transition from predominant Co^{2+} aqua ion speciation to adsorption on Fe_3O_4 NPs in the 200–250 °C temperature range.

Furthermore, the FT and the $k^3 \cdot \tilde{\chi}(k)$ data show that Co^{2+} begins to react with Fe_3O_4 nanoparticles around 250 °C. Our data show that adsorbed Co ion speciation on the surface of the Fe_3O_4 NPs predominant in the 250–500 °C temperature range in the sample, which is consistent with our published XANES data [21]. This is considerably different than our XAS results for the aqueous Ni-Fe_3O_4 NP system under high *P*–*T* conditions. The reaction temperature of Co^{2+} ions is between 100 °C and 150 °C lower than the reaction of Ni^{2+} ions with

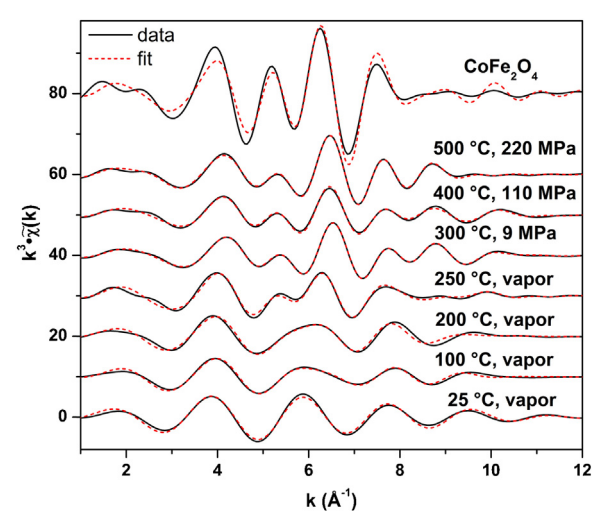

Fig. 6. Inverse Fourier transform $k^3 \cdot \chi(k)$ data (solid lines) calculated from Fourier transforms shown in Fig. 5 and the corresponding best fits to the data (dashed lines).

Fe_3O_4 nanoparticles under hydrothermal conditions [14]. For the aqueous Ni-Fe_3O_4 NP system, Ni aqua ion complexation strongly predominates to 300 °C whereas we see some evidence of Co ion adsorption at 100 °C and 200 °C (see Figs. 5 and 6).

The results from fitting of the Co *K*-edge EXAFS data are shown in Table 1. The estimated errors shown in Table 1 are the statistical uncertainties calculated during fitting of the XAS data using IFEFFIT. The O_{H_2O} label in Table 1 refers to the oxygen atoms in the Co^{2+} aqua ion speciation. The O_1, Fe_1, and Fe_2 labels in Table 1 refer to first-neighbor oxygen atoms, first-neighbor iron atoms, second-neighbor iron atoms, respectively, in the cluster based on the spinel phase (Fig. 2). The structural parameters (N, R, and σ^2) for O_{H_2O}, O_1, Fe_1, and Fe_2 were determined from fitting using only single scattering paths calculated using FEFF, which traverse from the target Co atom to the surrounding oxygen or iron atoms. Attempts at fitting of the EXAFS data using separate cluster models having the central atom (Co) either in a tetrahedral site (T_d in Fig. 2) or an octahedral site (O_h in Fig. 2) showed that the data are clearly best fit using the cluster model with the Co atom in the octahedral site. This is consistent with FEFF modeling of XANES data [21]. Fitting of the Co *K*-edge EXAFS data measured from bulk $CoFe_2O_4$ was made using the same single-scattering paths (O_1, Fe_1, and Fe_2) as for the Co-Fe_2O_4 NP•aq sample. However, because bulk $CoFe_2O_4$ is a partially inverse spinel with a high degree of inversion ($i = 0.77$), it was necessary to employ two single-scattering O_1 paths; one for Co occupation in tetrahedral sites and another for octahedral site occupation. The N and R structural parameters of bulk $CoFe_2O_4$ for O_1 shown in Table 1 are weighted averages of their respective quantities from the tetrahedral and octahedral Co site occupations.

The EXAFS data measured at 25 °C and vapor pressure were fit using a single oxygen shell. The coordination number ($N \approx 6$) result that was obtained from fitting is consistent with a predominant octahedrally coordinated Co aqua ion species. The EXAFS data measured at temperatures ranging from 100 °C to 250 °C show the transition from aqua ion speciation to predominant adsorption of Co^{2+} on Fe_3O_4 NPs in aqueous fluids. This is clearly observed from the decreasing coordination number (N) of O_{H_2O} whereas the N of O_1, Fe_1, and Fe_2 generally increase with temperature. The mixed speciation (aqua ion and adsorbed species) of Co in the 100–250 °C temperature range accounts for the reduced N values of O_{H_2O}, and the increased N values of O_1, Fe_1, and Fe_2. The bond length (R) of O_{H_2O} is consistently 0.12–0.14 Å longer than R of O_1 from 100 °C to 250 °C. In the 300 °C and 9 MPa to 500 °C and 220 MPa *P*–*T* range, analyses of the EXAFS data show that Co aqua ion speciation is negligible and that Co is predominantly chemisorbed on Fe_3O_4 NPs. This is evident in negligible N values of O_{H_2O} whereas N of O_1, Fe_1, and Fe_2 are greater in the 300–500 °C temperature range compared to the same coordination numbers at lower *P*–*T* conditions. The structure data shown in Table 1 for the 300–500 °C temperature range are in very good agreement with results obtained from XAS measurement of $CoFe_2O_4$ NPs by Carta et al. [27].

Cobalt ferrite has a partially inverted spinel structure with high degree of inversion where Co^{2+} predominantly occupies octahedral sites [28]. In all likelihood, the structural environment in Co-Fe_3O_4 NPs shows partially inverted spinel structure. Our data appear to indicate that the degree of inversion is somewhat higher than the results for cobalt ferrite nanoparticles reported by Carta et al. [27]. However, the cobalt ferrite nanoparticles in Ref. [27] are embedded in a silica gel matrix, which have a lower degree of inversion for sol–gel-derived cobalt ferrite compared to solid-state-derived $CoFe_2O_4$ NPs.

The mechanism of adsorption of metal ions on the surface of nanoparticles in aqueous fluids at high *P*–*T* conditions has not been elucidated. Furthermore, studies based on modeling of the adsorption of metal ions on nanoparticles are scarce. Phan et al. [29] have successfully used the triple layer model (TLM) in analysis of their data on Zn^{2+} adsorption on silica nanoparticles in aqueous solutions of varying pH values. The TLM has also been applied to modeling of the adsorption of Co^{2+} on bulk Fe_3O_4 by Crescenti and Sverjensky [30]. Modeling of the adsorption onto mineral surfaces in aqueous solutions typically involves accounting for outer sphere and inner sphere metal ion complexes. In the case of aqua ions, the inner sphere complex is partially hydrated and partially coordinated with one or more surface OH's whereas the fully hydrated outer sphere complex is coordinated to surface OH's via one or more of its inner sphere water molecules. Because our EXAFS data (Table 1) do not show structural parameters indicative of hydration (with R of O_{H_2O} ~2.10 A) and a second shell of oxygen atoms, we conclude that we do not have evidence for outer sphere Co^{2+} ion adsorption on Fe_3O_4 NPs. Our results are consistent with coexisting aqua ion speciation and inner sphere complex formation on the protonated Fe_3O_4 NP surface at temperatures ranging from 25 °C to 200 °C and surface incorporation, i.e., precipitation or chemisorption leading to $Co_xFe_{3-x}O_4$ ($x \leq 1$) surface phase formation, of Co^{2+} under higher *P*–*T* conditions, from 250 °C to 500 °C and vapor pressure to 220 MPa. The structural results for 250 °C (and vapor pressure) indicate transitional behavior most likely from inner sphere complexing to surface incorporation of Co^{2+} on Fe_3O_4 NPs. This is evident in the limited extended structure (low coordination with Fe_1 and no coordination with Fe_2) in the EXAFS to 200 °C and much stronger extended nanoparticle structure in the 250–500 °C range. This is consistent with our experiment showing that chemisorption of Co on Fe_3O_4 NPs occurs subsequent to hydrothermal treatment under high temperature conditions (370 °C) and not under lower temperature conditions (140 °C). In similar fashion to precipitation of Ni on Fe_3O_4 NPs reported by our group [14], our results suggest nominal inter-diffusion of Fe and Co in the surface region of Fe_3O_4 NPs (up to ~1 nm in extent) in aqueous fluids under high *P*–*T* conditions. This is primarily supported from the EXAFS results showing that the local structure (i.e., O_1, Fe_1, and Fe_2 coordination numbers) becomes more pronounced with increasing temperature in the 300–500 °C range.

The fact that the Co^{2+} aqua ion reacts at considerably lower temperatures than the Ni^{2+} aqua ion [14] is indicative of a lower chemisorption activation energy for Co^{2+} than for Ni^{2+} on Fe_3O_4 NPs in aqueous fluids under hydrothermal conditions. This is consistent with a lower value of the crystal field stabilization energy (CFSE) of Co^{2+} than of Ni^{2+} in octahedral site symmetry in spinels [31]. In addition to CFSE, other considerations such as size (i.e., steric) effects, electronic orbital (e.g., Co 3d and O 2s, 2p) interactions, structural distortions and/or disorder, and temperature dependent entropy most likely play a role in site selectivity and strength of chemisorption. The role of some of these elements is being addressed in first-principles electronic structure calculations of $CoFe_2O_4$ and other spinel ferrites [32,33]. However, further experimental and theoretical investigations are required to more fully understand the mechanism(s) responsible for site occupancy and adsorption/chemisorption of transition metal ions on the surface of Fe_3O_4 NPs in aqueous fluids to supercritical conditions.

Our results show that for applications to power reactors, Co^{2+} aqua ions will react with spalled ferrite nanomaterial in moderately low-pH (pH = 4.96) aqueous fluids at temperatures starting at about 250 °C. Conversely, our previous study showed that Ni^{2+} aqua ions will react with spalled ferrite nanomaterial in similar fluids at higher temperatures (400 °C and beyond) [14]. The reaction and chemisorption of Ni^{2+} and Co^{2+} with spalled ferrite nanomaterial enables effective removal of these corrosive product metal ions from transport within aqueous fluids of the primary cooling loop of power reactors. Because the dissolved corrosive product metal ions tend to lower the pH and enhance the corrosivity of aqueous fluids, their sequestration by chemisorption to spalled ferrite

Table 1
Structure results from fitting of EXAFS spectra measured from the Co-Fe_3O_4 NP•aq sample at different temperatures and the estimated pressures and from bulk $CoFe_2O_4$.[a]

	Co-Fe_3O_4 NPs							$CoFe_2O_4$
T (°C)	25	100	200	250	300	400	500	–
P (MPa)	Vapor	Vapor	Vapor	Vapor	9	110	220	–
N								
O_{H_2O}	6.1 (4)	4.3 (2)	4.7 (3)	4.0 (3)	–	–	–	–
O_1	–	2.0 (2)	2.0 (3)	2.0 (3)	3.9 (5)	4.4 (3)	4.6 (3)	6.1 (7)
Fe_1	–	1.9 (1)	2.5 (1)	5.4 (8)	6.0 (6)	6.2 (2)	6.8 (1)	6.0 (8)
Fe_2	–	–	–	3.1 (6)	3.2 (2)	3.6 (1)	3.9 (2)	8.9 (8)
R (Å)								
O_{H_2O}	2.10 (2)	2.12 (6)	2.10 (3)	2.10 (2)	–	–	–	
O_1	–	1.98 (3)	1.98 (4)	1.98 (1)	1.95 (1)	1.97 (2)	1.98 (2)	2.07 (4)
Fe_1	–	2.87 (3)	2.94 (4)	3.00 (5)	2.96 (2)	2.96 (3)	2.99 (2)	2.98 (1)
Fe_2	–	–	–	3.53 (5)	3.40 (2)	3.45 (4)	3.50 (6)	3.50 (1)
σ^2 (10^{-2} Å^{-2})								
O_{H_2O}	0.7 (1)	0.9 (3)	0.7 (3)	0.7 (2)	–	–	–	–
O_1	–	1.0 (3)	0.9 (3)	0.8 (4)	0.8 (1)	1.1 (2)	1.0 (2)	0.3 (2)
Fe_1	–	1.5 (3)	1.5 (4)	1.5 (3)	1.4 (1)	1.5 (1)	1.1 (1)	0.4 (1)
Fe_2	–	–	–	1.3 (6)	1.4 (3)	1.5 (3)	1.6 (5)	0.6 (2)
$\Re_{fit}$								
0.03	0.03	0.05	0.03	0.004	0.02	0.007	0.07	

[a] A O_{H_2O} signifies H_2O oxygen atoms of Co^{2+} aqua ion species; O_1 signifies first-neighbor oxygen atoms, Fe_1 first-neighbor iron atoms, and Fe_2 second-neighbor iron atoms surrounding the Co^{2+} ion adsorbed on Fe_3O_4 NPs. The estimated errors are at the 1σ confidence level and $\Re_{fit}$ is the goodness-of-fit parameter. The $X = N, R$ values of bulk $CoFe_2O_4$ for O_1 are weighted averages calculated using the formula $X = (i-1)\cdot X_{Td} + i\cdot X_{Oh}$, where X_{Td} and X_{Oh} the structural parameters for tetrahedral and octahedral Co site occupations, respectively.

nano- and very likely micro-material may help to lower the corrosivity in the primary cooling loop. It is plausible however that precipitation reaction of Co^{2+} and Ni^{2+} involve deprotonation at the surface of Fe_3O_4 nanoparticulates, resulting in a lowering of the pH of the high P–T aqueous fluid. The fate of ^{60}Co, a long lived isotope activated by neutron capture, is of particular concern in nuclear SCWRs. Our study suggests that a significant amount of ^{60}Co will be chemisorbed to the surface of spalled ferrite nanomaterial in the primary cooling loop of nuclear SCWRs. In addition, hydrothermal treatment of Fe_3O_4 and other NPs in the presence of metal ions may have applications for catalysis, particularly where cost of material is a factor (e.g., Pt), due to chemisorption of the metal ion within the catalytically active surface region of the nanoparticulate material.

4. Conclusions

Analysis of in situ EXAFS data show that the reactivity of the Co^{2+} aqua ion species with Fe_3O_4 NPs is minimal up to 200 °C but becomes significant in the aqueous fluid from 250 °C to 500 °C. Our results are consistent with coexisting Co^{2+} aqua ion and inner sphere complex species that are adsorbed on the surface of Fe_3O_4 NPs from 25 °C to 200 °C and predominantly chemisorbed (i.e., precipitated) Co^{2+} ions on Fe_3O_4 NP surface sites from 250 °C to 500 °C, in the nanoparticle-aqueous-fluid sample. The Co^{2+} ion is preferentially chemisorbed on octahedral sites, consistent with inverse spinel structure, on Fe_3O_4 NPs in aqueous fluids from 250 °C to 500 °C. Detailed structural results from EXAFS analysis are consistent with diffusion of Co into the first few atomic layers of the near-surface region of the Fe_3O_4 NPs in the aqueous fluids under high P–T conditions. Our results suggest that the dissolved radioactive isotope ^{60}Co will be precipitated on spalled ferrite nanomaterial within the primary cooling loop of nuclear SCWRs.

Acknowledgments

H.Y. and R.A.M. were supported as part of the EFree, an Energy Frontier Research Center funded by the U.S. Department of Energy, Office of Science, Office of Basic Energy Sciences under Award Number DE-SC0001057. A.J.A. was supported by an NSERC/NRCan/AECL Generation IV Collaborative Research Development (CRD) grant. The PNC/XOR facilities at the APS, and research at these facilities, are supported by DOE-BES, a Major Resources Support (MRS) grant from NSERC, the University of Washington, Simon Fraser University and the Advanced Photon Source. Use of the Advanced Photon Source is also supported by DOE-BES, under Contract DE-AC02-06CH11357. We are thankful to Steve Heald, Robert Gordon and staff of PNC/XOR for assistance with our XAS experiments and to Kai Song and the Advanced Materials Characterization Laboratory at Missouri University of Science and Technology for TEM characterization. We thank the anonymous referees for constructive comments that helped to improve this paper.

References

[1] Basic Research Needs for Materials Under Extreme Environments, Report of the Basic Energy Sciences Workshop for Materials under Extreme Environments, DOE, 2007.
[2] D. Guzonas, SCWR materials and chemistry status of ongoing research: the generation IV international forum (GIF) symposium, in: Proceedings of the GIF Symposium, Paris, France, 2009, p. 163.
[3] R. Viswanathan, J. Sarver, J.M. Tanzosh, Boiler materials for ultra-supercritical coal power plants—steamside oxidation, Journal of Materials Engineering and Performance 15 (2006) 255–274.
[4] R.W. Shaw, T.B. Brill, A.A. Clifford, C.A. Eckert, E.U. Franck, Supercritical water: a medium for chemistry, Chemical & Engineering News 69 (1991) 26–39.
[5] P. Kritzer, Corrosion in high-temperature and supercritical water and aqueous solutions: a review, Journal of Supercritical Fluids 29 (2004) 1–29.
[6] Nanostructured Coatings; EPRI Report 1014805.
[7] C. Sun, R. Hui, W. Qu, S. Yick, Progress in corrosion resistant materials for supercritical water reactors, Corrosion Science 51 (2009) 2508–2523.
[8] Y. Jun, J.-H. Lee, J. Cheon, Chemical design of nanoparticle probes for high-performance magnetic resonance imaging, Angewandte Chemie International Edition 47 (2008) 5122–5135.
[9] C. Sun, J.S.H. Lee, M. Zhang, Magnetic nanoparticles in MR imaging and drug delivery, Advanced Drug Delivery Reviews 60 (2008) 1252–1265.
[10] A. Tomitaka, M.-H. Jeun, S.-T. Bae, Y. Takemura, Evaluation of magnetic and thermal properties of ferrite nanoparticles for biomedical applications, Journal of Magnetics 16 (2011) 164–168.
[11] E.J.W. Verwey, E.L. Heilmann, Physical properties and cation arrangement of oxides with spinel structures I. Cation arrangement in spinels, Journal of Chemical Physics 15 (1947) 174–180.
[12] K.E. Sickafus, J.M. Wills, N.W. Grimes, Structure of spinel, Journal of the American Ceramic Society 82 (1999) 3279–3292.
[13] J. Smit, Ferrites, Physical Properties of Ferrimagnetic Oxides in Relation to Their Technical Applications, Philips Technical Library, 1959.

[14] R.A. Mayanovic, H. Yan, A.J. Anderson, P.R. Meredith, W.A. Bassett, In situ X-ray absorption spectroscopic study of the adsorption of Ni^{2+} on Fe_3O_4 nanoparticles in supercritical aqueous fluids, Journal of Physical Chemistry C 116 (2011) 2218–2225.
[15] B.E. Warren, X-ray Diffraction, Dover Publications Inc., 1990.
[16] R.A. Mayanovic, A.J. Anderson, W.A. Bassett, I.-M. Chou, Synchrotron X-ray spectroscopy of Eu/HNO_3 aqueous solutions at high temperatures and pressures and Nb-bearing silicate melt phases coexisting with hydrothermal fluids using a modified hydrothermal diamond anvil cell and rail assembly, Review of Scientific Instruments 78 (2007) 053904.
[17] I.-M. Chou, W.A. Bassett, A.J. Anderson, R.A. Mayanovic, L. Shang, Containment of fluid samples in the hydrothermal diamond-anvil cell without the use of metal gaskets: performance and advantages for in situ analysis, Review of Scientific Instruments 79 (2008) 115103.
[18] H. Yan, R.A. Mayanovic, A.J. Anderson, P.R. Meredith, An in situ X-ray spectroscopic study of Mo^{6+} speciation in supercritical aqueous solutions, Nuclear Instruments and Methods in Physics Research Section A: Accelerators, Spectrometers, Detectors and Associated Equipment 649 (2011) 207–209.
[19] W. Wagner, A. Pruß, The IAPWS formulation 1995 for the thermodynamic properties of ordinary water substance for general and scientific use, Journal of Physical and Chemical Reference Data 31 (2002) 387–535.
[20] A.L. Ankudinov, B. Ravel, J.J. Rehr, S.D. Conradson, Real-space multiple-scattering calculation and interpretation of X-ray-absorption near-edge structure, Physical Review B 58 (1998) 7565–7576.
[21] H. Yan, R.A. Mayanovic, J. Demster, A.J. Anderson, In situ XANES study of Co^{2+} ion adsorption on Fe_3O_4 nanoparticles in supercritical aqueous fluids, in: MRS Online Proceedings, 2012, p. 1383, mrsf11-1383-a07-10.
[22] F. Farges, Ab initio and experimental pre-edge investigations of the Mn *K*-edge XANES in oxide-type materials, Physical Review B 71 (2005) 155109.
[23] L. Hedin, B.I. Lundqvist, Explicit local exchange-correlation potentials, Journal of Physics C: Solid State Physics 4 (1971) 2064–2083.
[24] B. Ravel, M. Newville, Athena, artemis, hephaestus: data analysis for X-ray absorption spectroscopy using IFEFFIT, Journal of Synchrotron Radiation 12 (2005) 537–541.
[25] M. Newville, IFEFFIT: interactive XAFS analysis and FEFF fitting, Journal of Synchrotron Radiation 8 (2001) 322–324.
[26] G. Dräger, R. Frahm, G. Materlik, O. Brümmer, On the multipole character of the X-ray transitions in the pre-edge structure of Fe K absorption spectra. An experimental study, Physica Status Solidi (b) 146 (1988) 287–294.
[27] D. Carta, G. Mountjoy, G. Navarra, M.F. Casula, D. Loche, S. Marras, A. Corrias, X-ray absorption investigation of the formation of cobalt ferrite nanoparticles in an aerogel silica matrix, Journal of Physical Chemistry C 111 (2007) 6308–6317.
[28] A.S. Vaingankar, B.V. Khasbardar, R.N. Patil, X-ray spectroscopic study of cobalt ferrite, Journal of Physics F: Metal Physics 10 (1980) 1615–1619.
[29] T.N.T. Phan, N. Louvard, S.-A. Bachiri, J. Persello, R. Foissy, Adsorption of zinc on silica, triple layer modelisation and aggregation data, Colloids and Surfaces A: Physicochemical and Engineering Aspects 244 (2004) 131–140.
[30] L.J. Crescenti, D.A. Sverjensky, A single-site model and for divalent transition and heavy metal adsorption over a range of metal concentrations, Journal of Colloid and Interface Science 253 (2002) 329–352.
[31] R.G. Burns, Mineralogical Applications of Crystal Field Theory, 2nd ed., Cambridge University Press, 1993.
[32] Y.H. Hou, Y.J. Zhao, Z.W. Liu, H.Y. Yu, X.C. Zhong, W.Q. Qiu, D.C. Zeng, L.S. Wen, Structural, electronic and magnetic properties of partially inverse spinel $CoFe_2O_4$: a first-principles study, Journal of Physics D: Applied Physics 43 (2010) 445003.
[33] Z. Szotek, W.M. Temmerman, D. Ködderitzsch, A. Svane, L. Petit, H. Winter, Electronic structures of normal and inverse spinel ferrites from first principles, Physical Review B 74 (2006) 174431.